Melanoma Recognition in Dermoscopy Images Using Lesion's Peripheral Region Information

Neda Zamani Tajeddin , Babak Mohammadzadeh Asl

PII: S0169-2607(17)31325-1
DOI: 10.1016/j.cmpb.2018.05.005
Reference: COMM 4702

To appear in: *Computer Methods and Programs in Biomedicine*

Received date: 28 October 2017
Revised date: 17 April 2018
Accepted date: 3 May 2018

Please cite this article as: Neda Zamani Tajeddin , Babak Mohammadzadeh Asl , Melanoma Recognition in Dermoscopy Images Using Lesion's Peripheral Region Information, *Computer Methods and Programs in Biomedicine* (2018), doi: 10.1016/j.cmpb.2018.05.005

Highlights:

- A high precision system for melanoma recognition based on dermoscopic images.
- Limiting the complex texture features to the lesion area only.
- Introducing a set of features based on the log-polar transformation of the lesion's peripheral region.
- New features do not need further segmentation of dermoscopic structures and are robust against lesion's scale, orientation, location, and shape variation.
- Incorporating two classifiers: one for melanoma vs. nevus recognition, another for melanoma vs. nevus and atypical nevus recognition.
- Conducting feature selection experiments in order to find the most discriminative feature set.

Melanoma Recognition in Dermoscopy Images Using Lesion's Peripheral Region Information

Neda Zamani Tajeddin, Babak Mohammadzadeh Asl*

ABSTRACT

Background and Objectives: Melanoma is one of the most dangerous forms of skin cancer, but it has a high survival rate if diagnosed on time. The first diagnostic approach in melanoma recognition is to visually assess the lesion through dermoscopic images. Computer-aided diagnosis systems for melanoma recognition has attracted a lot of attention in the last decade and proved to be helpful in that area. Methods for skin lesions analysis usually involves three main steps: lesion segmentation, feature extraction, and features classification. Extracting highly discriminative features from the lesion has a great impact on the recognition task. In this paper, we are seeking a lesion recognition system that incorporates these highly discriminative features. ***Methods:*** For segmentation step, we use contour propagation model with a novel two-component speed function. In the feature extraction step, a new set of features based on peripheral information of the lesion are introduced. For this end, the peripheral area of the lesion is mapped to log-polar space using the Daugman's transformation and then a set of texture features are extracted from it. Newly introduced features do not need further segmentation of dermoscopic structures and are robust against lesion's scale, orientation, location, and shape variation. We also design the other global texture features to describe only the information from the lesion area. In the classification step, we evaluated two different schemes to prove the distinction power of the new features, one comprises linear SVM to recognize melanoma vs. nevus and the other scheme uses RUSBoost classifier to recognize melanoma vs. nevus and atypical-nevus. Sequential feature selection algorithm has been utilized in each classification scheme to rank features based on their distinction power. ***Results:*** Cross-validation experiments on the well-known PH^2 dataset resulted in an average of 97% for sensitivity and 100% for specificity on melanoma vs. nevus recognition task using only four features. Also, in the second classification scheme, we achieved high sensitivity and specificity values of 95% for melanoma vs. nevus and atypical nevus recognition experiments. ***Conclusion:*** High values for evaluation metrics show that the proposed melanoma recognition system is superior to the other state-of-the-art algorithms, which proves the high distinction power of the newly introduced features.

Keywords: Melanoma; feature extraction; lesion peripheral information; Daugman rubber sheet model.

* Corresponding author.
The authors are with the Department of Biomedical Engineering, Faculty of Electrical and Computer Engineering, Tarbiat Modares University, Jalal Ale Ahmad, P.O.Box: 14115-111, Tehran, Iran.
Email addresses: n.zamanitajeddin@modares.ac.ir (Neda Zamani Tajeddin), babakmasl@modares.ac.ir (Babak Mohammadzadeh Asl)

1. Introduction

One of the most dangerous forms of the skin cancer is melanoma. It is usually more common in people living in rural and remote regions. Unfortunately, access to specialists for these people is harder than the others. Based on official statistics, in the year 2017, nearly 87,110 people in the United States of America are estimated to diagnose with melanoma, and about 9,730 of them are expected to die in 2018 [1]. Despite the high number of patients worldwide, melanoma has a good survival rate if diagnosed on time, e.g., it has a survival rate of 86% in Great Britain and more than 90% in USA over recent five years [2].

Shape, color, or texture of the lesion in melanoma cases would differ from a normal nevus. Irregular edges, more than one color, itching or bleeding are other symptoms of lesions diagnosed with melanoma. Usually, dermatologists use two well-known criterions to visually evaluate a skin lesion and diagnose it as a melanoma, one is ABCD rules and the other one is 7-point checklist [3]. Each of initial letters in ABCD rules stand for a clinical criterion to assess the appearance of the lesion: rule A characterizes the asymmetries in lesion's shape (or appearance), B rule indicates the border irregularities, C rule refers the color properties of the lesion, and D rule measures the diameter of the lesion [4,5]. In the recent years, the 7-point checklist has attracted more attention for melanoma recognition. It comprises a list of seven items (symptoms of melanoma) with a companion score. Three items (atypical pigment network, blue-whitish veil, and atypical vascular pattern) are considered as major criteria and have 2 scores, remaining four items (irregular streaks, irregular pigmentation, irregular dots/globules, and regression pattern) are considered minor criterions and assigned 1 score each. Based on this list's criterions, if a lesion assigned with three or more points, it is considered as a melanoma case [5,6].

Dermatologists often inspect skin lesions visually using a dermatoscope. Fortunately, these devices can be coupled to smartphones and other handheld devices to raise the ability of melanoma inspection in remote areas. Using computer-aided diagnosis (CAD) systems alongside with these mobile devices can help realizing an automatic skin lesion classification system which hopefully would lead to higher rates in melanoma recognition, especially in rural areas where access to a dermatologist is more difficult. CAD systems with the use of image processing methods can also assist dermatologists to achieve a better diagnosis.

Image processing methods for skin lesions analysis usually involve three main steps after preprocessing: lesion segmentation, feature extraction, and features classification. Deficiencies like hair occlusion, uneven illumination, and dark corners usually exist in dermoscopic images. Due to these deficiencies, preprocessing is a vital task before any further analysis. There is a vast variety of methods proposed to solve each of these problems [4–6].

After preprocessing the first step in the skin lesion image analysis is to detect the lesion border from the other regions of skin. Generally, segmentation methods used in the field of skin lesion analysis can be

categorized into thresholding, region, edge, neural network, or active contour based algorithms [8]. However, we used the method in our previous work [8] to carry out the segmentation step.

The second step in the general melanoma recognition framework is to extract features from lesion's image. There are several ways to categorize the extracted features. One may categorize them based on the clinical definition of lesion's features e.g., putting a specific feature like lesion's diameter into one of the four criterions of the ABCD rules or an item of the 7-point checklist [10]. But usually in the field of skin lesion image analysis, the features are categorized into different groups based on the property that they refer to (like lesion's shape, color or texture) and the region that they have been extracted from (global features which are extracted from the whole area of the lesion or local features extracted from local regions of it) [4,11,12].

Anyway, it is for sure that with more discriminative features the recognition system will work better. Thus, a lot of researchers put their efforts in this area and tried to introduce new discriminative features. Most of the recent successful approaches used local features [12–14] or proposed to extract features that describe special dermoscopic structures e.g., streaks, pigment networks, or blue-whitish veils [15–18]. The latter group of works usually need to segment each particular structure previous to extract discriminative features from them, which makes that algorithms hard to implement and generalize. However, in this paper, we also have emphasized on the feature extraction step in order to improve the melanoma recognition.

After the feature extraction phase, extracted features are passed into a classification system in order to complete the general recognition framework. At this stage, classification system can be a single classifier or an ensemble of classifiers [19].

The main contribution of this paper lies within the feature extraction step. A new set of features are proposed based on the peripheral region of the lesion. First, the peripheral area of the lesion is mapped to log-polar space using the Daugman's transformation [20] and then a set of texture features is extracted from it. Newly proposed features are able to describe the appearance of the peripheral region and implicitly characterize the distribution of the streaks in that region. Unlike the methods in [15–18], our proposed framework does not need any further segmentation or detection of special dermoscopic structures and it is robust against lesion scale, rotation, and shape variation. We also explained how to precisely limit the other global features (like texture features) to the lesion area information only. In this paper, we used the linear variant of the Support Vector Machine (SVM) classifier [21] to classify the extracted features in a melanoma vs. nevus scheme and in another classification scheme, a Random Under-Sampling Boosted (RUSBoost) classifier [22] has been utilized to recognize melanoma samples from nevus and atypical nevus. In all classification scenarios, a sequential feature selection (SFS) framework based on cross-validation experiment has been used to search for the optimal feature subset and elevate the classification performance.

Rest of the paper is arranged as follows: in section 2, we would briefly review the related research in the field of melanoma recognition. Section 3 will describe the general lesion recognition methodology which comprises our implemented preprocessing, segmentation, feature extraction, and classification steps. Features described in section 3 are mostly adopted from the previous works but modified to only comprises lesion area information. Section 4 explains the newly introduced features in detail. The experimental results of applying the proposed methods on the available dataset and discussion related to that are presented in sections 5 and 6, respectively. Finally, the paper is concluded in section 7.

2. Related works

There is a vast literature on skin lesion segmentation methods [8]. Silveira et al. proposed several methods for skin lesion segmentation in [6]: adaptive thresholding, gradient vector flow, adaptive snake, level set method, EM-based level set method, and a fuzzy-based split and merge algorithm. They showed that adaptive snake algorithm performs the best on the PH^2 dataset [6]. Pennisi et al. [22] used Delaunay triangulation for melanoma detection, they portioned the image into several regions and decide which region belongs to the lesion. Barata et al. [11] and Abbas et al. [24] used thresholding based methods to segment the lesion. Barata et al. [11] chose the threshold based on the image histogram but Abbas et al. [24] take an iterative thresholding approach and also incorporated active contours to refine the segmentation output. Cavalcanti et al. [25] proposed a new channel that has the lesion enhanced in it, this way they were able to initially segment the lesion by applying a threshold on that channel and then they refined the results using active contours. In a recent work, Jahanifar et al. [26] proposed a supervised saliency detection algorithm, specially tailored for dermoscopic images, in order to detect the lesion. All of the mentioned methods have incorporated some relevant pre and post-processing measures to elevate the segmentation results. For more comprehensive reviews on dermoscopic image preprocessing and segmentation techniques refer to [3–7].

There is a tremendous number of features proposed in the literature to describe the shape, color, or texture of the lesions. Describing all of them is beyond the scope of this paper but for a general review on this topic, we invite the readers to refer to [4,10,12]. Here we review the works that used features extracted from local regions of the lesion. Barata and her coworkers introduced bag-of-features framework [11,14] to extract textural and color features from different patches of the image located at specific points on the lesion's area, called "keypoints". They showed that collecting appearance information from local regions of the lesion can increase the melanoma recognition rate [11,14]. These recognition systems are very sensitive to selecting appropriate number and location for the keypoints.

Celebi et al. [18] propose to detect regions of the image with blue color as an indicator of blue-whitish veils, which is a direct rule in the 7-point checklist. In a recent work, Maglogiannis et al. [17] introduced

new features based on dark dots and globules structures. For that, in addition to the lesion mask, the segmentation of dot/globules is needed, which is very difficult to achieve [17]. There are some researches that described other dermoscopic structures like streaks in [15] and pigment networks in [16]. These methods need to segment their target structures, which is a difficult task that adds extra complexity to the analysis of the lesion. In addition to difficulty, these segmentation methods are very prone to errors and also there is not enough annotated dataset available regarding these problems.

In the literature of melanoma recognition, different classifiers have been used that some of the most popular of them are support vector machines (SVMs), k-nearest neighbors (KNNs), Bayesian classifier, decision trees, and artificial neural networks (ANNs) [4,5]. Pennisi et al, used Adaboost classifier in their works [22,26]. Barata et al. proposed a method based on the dictionary learning in [14] and another one based on the SVM classifier in [10] (which has been announced as the benchmark method for the PH^2 dataset [28]). For a more comprehensive review of the classification methods used for melanoma recognition please refer to [4,6,11].

3. Lesion recognition methodology

The overview of the implemented method for melanoma recognition is described in the block diagram of Fig. 1. Besides the preprocessing, the whole recognition process consists of three main steps: lesion segmentation, feature extraction, and feature classification (which is coupled with feature selection in training phase). In the following subsections, we will describe each part in details.

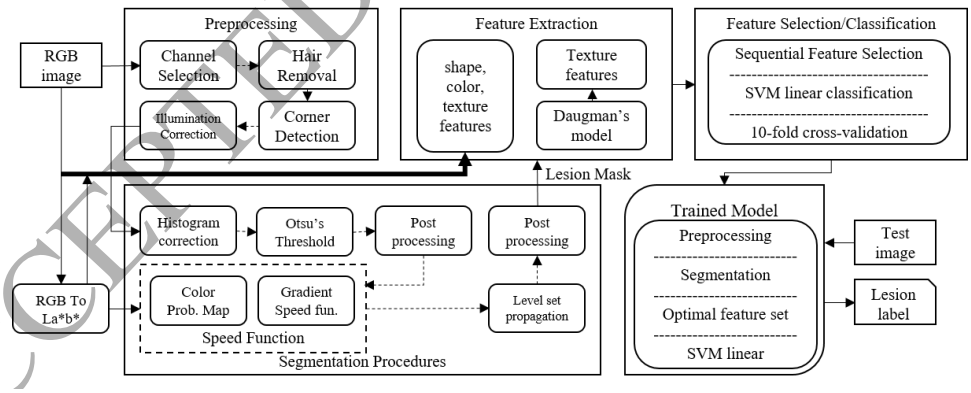

Fig. 1. Schematic of the proposed method for melanoma lesion recognition

3.1. Preprocessing

Our preprocessing step comprises four different tasks which are channel selection, hair and ruler marker inpainting (hair removal), eliminating dark corner effect (corner detection), and image uneven illumination correction. All of these steps are described thoroughly in [8] and here we just introduced them briefly. First, we select a channel from the image that has the most entropy to be used in further

operations [6]. Next, hairs and ruler marks are detected and inpainted using DullRazor filter [28]. Knowing that the image capturing situation is the same for all samples in the current dataset, we do not need to define or obtain a new corner mask for each image and we can just use a constant border mask for all images, as Silveira *et al.* did in [6]. To correct uneven illumination, homomorphic filtering [38] is used. To implement homomorphic filtering on an RGB image, we first transform the image from RGB space to La*b* space, perform homomorphic filtering on L component of it and then transform the manipulated La*b* image back to RGB space. It has been seen that homomorphic filtering corrects the uneven illumination and increases the image contrast as well.

3.2. Segmentation process

For the segmentation purpose, we use the same method proposed in [8]. The segmentation process consists of two main steps: construction of an initial mask and propagating the initial mask toward lesion boundary. For the first step, histogram of the selected channel is corrected to eliminate the effect of dark corner pixels on the histogram counts [8]. Then, the Otsu's method [30] is applied on the corrected histogram to obtain an appropriate threshold and construct a thresholded binary mask. We apply a series of post-processing tasks, mostly morphological operations, on the thresholded output mask to obtain the initial lesion mask. Usually, the initial mask does not delineate the lesion's boundary good enough. Thus, we propose to propagate the contour of the initial mask toward the real boundary of the lesion using Malladi *et al.* [31] approach. A dual-component speed function that can better guide the initial contour toward the lesion boundaries is used in that approach. This speed function uses a combination of original gradient based component and a new color (region) based component [8].

3.3. Feature extraction

Dermatologists look for some specific visual features in the lesion to recognize its type. A CAD system with the same goal must be able to extract those appearance features to decide about lesion type. With more discriminative features, there will be a higher chance to achieve a correct lesion type recognition.

In this research, we propose to extract shape, color, and texture related features from all areas of the lesion (general features), as well as some texture features from the only peripheral regions of it (local features). As for the latter task, we propose a new framework based on Daugman's rubber-sheet model [11] to transform the peripheral region of the lesion into a log-polar space and then extract some discriminative texture features from it. We will explain this novel framework for local feature extraction in the next section, but in the following subsections, the general features are described in more details. General features can be extracted from the image information of the region specified by the lesion mask, which is obtained in the segmentation step.

3.3.1. Shape related features

Shape features are describing the geometry of the lesion. Most of the items in ABCD rules can be implied as shape features. Area, perimeter, diameter, solidity, extent, and circularity of the lesion (6 features) are some examples of simple shape features [26]. But, there are more sophisticated features that are able to describe the lesion border and its specification more precisely.

a) Normalized Radial Length (4 features)

Normalized radial length (NRL) function is a shape descriptor that is used to extract some high-level shape features, like shape smoothness and roughness. We use these features to describe the border irregularities and imply the B item from ABCD rules. To extract the NRL related features, we must first define the NRL function itself. For the first step, a number of points are sampled on lesion boundary and the coordinate of the lesion centroid is calculated as well. The NRL function then can be defined as the normalized distance of each point to the lesion centroid [27]. Having the NRL function, we can define desirable shape features like average normalized radial length, the standard deviation of NRL, roughness index of the boundary, and smoothness index of boundary [27].

b) Asymmetry of shape (2 features)

Asymmetry assessment is the first rule of ABCD criterions and is a very important feature for melanoma recognition [28]. We assessed the border asymmetry using the two features proposed in [29]. In overall, considering aforementioned features, 12 shape features were extracted.

3.3.2. Color related features

Color specifications of the lesion play an important role in melanoma recognition. Considering color features alongside shape and texture features proved to be very efficient and elevate the classification accuracy [11,33,34]. Based on our review of the recent researches, we suggest using the following color features:

a) Statistical color measures (12 features)

This class of color features uses four first statistical moments (mean, standard deviation, skewness, and kurtosis) plus two other metrics (smoothness and SNR) on color channels of the image. The important note is to implement these metrics on appropriate color channels. Some researchers used RGB color channels to represent and calculate the color features of the lesion [34]. It has been known that these color channels are very sensitive to illumination variation [8]. We propose to first transform the image from RGB space to La*b* space, and then use a*, b* channels to describe the color of the lesion.

Consider $\Omega \in \mathbb{R}^2$ comprises all pixel positions that belong to the lesion. The color information of the lesion area in each image channel I_c can be represented as a vector: $\mathbf{x} = I_c(\Omega)$ where $c \in \{a^*, b^*\}$. Based

on this notation, we define the color features as the average, standard deviation, skewness, kurtosis, smoothness, and Signal to Noise Ratio (SNR, which is equal to average divided by standard deviation) of the $\mathbf{x}$ color vector.

b) Six-color model (7 features)

Different structures in lesion may have different colors, i.e. pigment networks with brown and black colors, streak patterns with red color, and blue-whitish veil with blue to gray color. Based on clinical studies [32,35], we can assume the appearance of six main colors in the skin lesion which are: black, dark-brown, light-brown, gray-blue, red, and white. Depending on how much lesion permeates into the skin, it can show different colors in different regions.

To assess the lesion color from this perspective, we propose a simple six-color model. In this model, we calculate the contribution of each mentioned color in the construction of the lesion color map as a percentage of whole lesion area. Each mentioned color has a specific range of the color spectrum. We translate that range from RGB space into La*b* space, and use the range of a*, b* instead. Apart from the contribution percentage of each main colors in the construction of the lesion (6 features), we propose to use the number of prominent colors. Each color that has a contribution percentage more than a certain threshold can be considered as a prominent color. Higher thresholds would lead to more confident, but less specific, prominent color detection. On the contrary, low threshold values would lead to more noisy detection. In order to have a high specificity in prominent color detection and avoiding noisy detections, we set the contribution threshold equal to 5 percent, empirically.

Extracting 6 statistical features from two different color channels would leave us with 12 color features. Adding 7 features extracted based on the six-color model, we would have 19 features describing the color of the lesion.

3.3.3. Texture related features

Lesion texture provides valuable information for classification. Shape and color features alone may not be discriminative enough to separate benign and malignant lesions from each other because it is very common that these two types of lesion represent the same shape or color features. But, combining these features with texture features proved to be very helpful in melanoma recognition [10,13]. All texture-related features in this work are extracted from the luminance component (L channel) of La*b* color space because its contents show more distinction in lesions textural structures. Another important issue is that texture features must describe only the texture of the lesion in the image, not other components of the image (like healthy skin, dark corners or color charts). So, we should take some measures to extract the texture features from the pixels that belong only to the lesion's area.

a) Statistical texture measures (8 features)

The statistical texture features (STFs) are widely used to describe the texture of the object of interest because they are simple and very easy to extract. To extract STFs, we must first construct the histogram from the image. It is very important to limit the values of the histogram bins to the constituent pixels of the lesion. With $\Omega(x, y)$ specifying the pixels that construct the lesion region in the L channel, we can define the lesions histogram as $\mathbf{H} = \{h_i \; ; i = 1,..., l\}$, in which i is the possible pixel values in the image, l is the length of the histogram and the highest pixel value in the image, and h_i is the pixel count. Having the histogram of pixels in the lesion's region we can easily extract 8 different STFs. Five of these features are mean, standard deviation, skewness, kurtosis, and smoothness of histogram information. The other three STFs are energy, entropy, and noise of histogram values that are defined as below:

- Energy of lesion's histogram values

$$\text{Energy}(\mathbf{H}) = \sum_{i=1}^{l} |h_i|^2 \quad (1)$$

- Entropy of lesion's histogram values

$$\text{Entropy}(\mathbf{H}) = -\sum_{i=1}^{l} h_i^2 \log(h_i^2) \quad (2)$$

- Noise of lesion's histogram values

$$\text{Noise}(\mathbf{H}) = \text{Energy}(\mathbf{H} * \mathbf{L}), \quad (3)$$

where $\mathbf{L}$ stands for Laplace operator and is defined as $\mathbf{L} = [-1 \;\; 2 \;\; -1]$ and $\mathbf{H} * \mathbf{L}$ is the convolution between the histogram signal and the Laplace operator. Finally, to estimate an extent of noise in the histogram, the energy of the resultant convolution is calculated based on (1). The above-introduced features can indirectly and efficiently imply that the texture of a lesion surface is smooth, noisy, seamless or irregular in terms of intensity variation.

b) Energy of Laws' filters responses (14 features)

Law's energy features (LEFs) emphasize on edge, spot, ripple, and wave structures in the texture of the image. Each of Laws' texture descriptors is defined based on five basic operators [36]. By combining these five operators with each other (through matrix multiplication) 14 different Law's descriptors can be made (list of all descriptors can be found in [36]). Graphical visualization of Laws' filter kernels is illustrated in Fig. 2, as one can see each descriptor targets a specific textural structure. After filtering the lesion image with each of 14 Law's descriptors, we obtain 14 filter responses in each of them a particular textural structure is highlighted. We compute the energy of pixels belonging to each of these filter responses, from only the lesion area, to construct a texture descriptor. We have 14 filter responses, so we would have 14 different filter response energies which can be used as texture features.

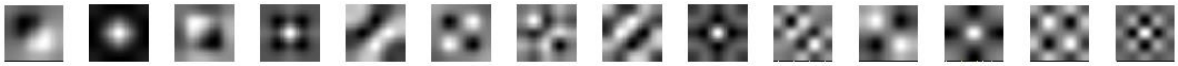

Fig. 2. Laws' filter bank: collection of 14 feature descriptors as defined in [36] **(interpolated to size 50x50).**

c) Gray-level co-occurrence matrix features (24 features)

A Gray-Level Co-occurrence Matrix (GLCM) represents the rate of appearance of two pixels with specific values which are in a particular ordering. GLCM features have been used as main textural features in most recent melanoma recognition studies [11,13], [16], [10], [37]. The procedure of expressing an image texture using GLCM has two stages: construction of GLCM and extracting texture-related features from GLCM.

GLCM is a square matrix the elements of which are the occurrence frequencies of a pixel pair with specific values, distance, and angle relative to each other. In this article, we quantize pixel values to 64 different gray levels and construct four different GLCM in four different angles with a constant distance parameter. As we said before, it is very important to constraint the extracted feature to the region of the lesion in the image. To do so for the GLCM features, we first mask the gray-level image with the binary lesion mask obtained from segmentation phase. Therefore, we have a gray-level image with all pixels zeroed outside the lesion area. We construct the GLCM from this masked image. Based on the fact that there are no absolute zero valued pixels in the real dermoscopic images, we can correct the GLCM for the absolute back region of the mask. This can be realized by setting the first element of GLCM to zero.

After construction of the GLCM, we can extract descriptive texture features from it. There are several features extracted from G LCM in the literature, in this research we use 24 textural features based on [38–40] named as: maximal probability, contrast, angular second moment, inverse difference moment, sum of squares, homogeneity (2 features), entropy, energy, sum average, sum entropy, sum variance, difference variance, difference entropy, informational measure of correlation (2 features), cluster tendency, cluster shade, cluster prominence, dissimilarity, correlation (2 features), autocorrelation, and maximum correlation coefficient. For all four constructed GLCMs, we compute the above-mentioned features (4x24 features) and finally, we average the features across different angles to obtain 24 features describing the texture of the lesion.

3.4. Classification and features selection process

Besides the discrimination power of the extracted features, the performance of the recognition greatly depends on choosing a suitable classifier. In this research, based on classification schemes that have been experimented on the available data we plan to use either linear SVM classifier [21] or RUSBoost classifier [22]. Using well-known linear SVM classifier makes it possible to compare the performance of only proposed features with the performance of the features proposed in the other works in a fair situation and RUSBoost classifier will be appropriate when the population of classes is more imbalance (more

details about the reasons that these classifiers have been chosen is described in the results section). Since the number of samples in the available dataset is limited and also to avoid overfitting in classification experiments, we evaluate the proposed method in a 10-fold cross-validation framework.

In order to select an optimal subset of features and determine the order of distinction power of each feature, we propose to conduct feature selection experiment as well. There are different methods to do this task, we prefer to utilize sequential feature selection (SFS) approach. SFS is an embedded based feature selection algorithm that uses a classifier to evaluate the performance of different combinations of the input features [42]. Based on SFS, feature selection pipeline used in this research is described as follow [42]: First, the performance of each feature is evaluated in a 10-fold cross-validation framework. The feature with best evaluation metric is selected as the first member of optimal feature subset and has the highest importance (distinction power) between all features. Then, by pairing the first selected feature with the other remaining features, groups of features with two members are constructed and evaluated in the same way and the best-performed group is selected. That two-membered group is joint with other features to form groups of three features and the evaluation is conducted on them as well. This procedure continues until the final group of features would comprise all of the available features. SFS is a suboptimal approach to find the best groups of features, but it is much more efficient than brute force complete search algorithms.

4. Proposed framework for extracting features from peripheral areas of the lesion

Studying the peripheral region of the lesion plays an important role in clinical recognition of melanoma. Usually in melanoma cases, color and texture of the lesion in the central region differ from that in the peripheral region [15]. Also, one of the most helpful dermoscopic features in melanoma recognition is the pattern of the streaks which are usually observed in outer regions.

In this research, we propose a new set of features based on the peripheral region in which, unlike [15], no further segmentation of dermoscopic structures is needed. We first determine the peripheral region based on the distance function obtained from the segmented binary mask of the lesion. Then, in a novel fashion, we map the peripheral lesion from Cartesian coordinate to a pseudo polar coordinate using Daugman's rubber sheet model [20]. Finally, several textural features are extracted from the projected peripheral region to represent its appearance and implicitly analyzing the dermoscopic structures in that region. In the following, we will investigate each of these steps more thoroughly.

4.1. Specifying the peripheral region

For this part of processing, we take the approach introduced in [15]. First, the lesion is rotated in the amount of its general orientation angle, so its major axis would be aligned horizontally with image axes.

Also, the bounding box of the lesion mask is used to crop the image and its mask, so the image would only comprise the lesion in the center of it.

To determine the peripheral region, we compute the distance function from the lesion mask. The peripheral region is a collection of pixels that are closer to the lesion boundary. So, we specify that region by thresholding the obtained distance function, we set this threshold equal to a quarter of lesion's minor axis length. Results of this process for a sample lesion mask is illustrated in Fig. 3. Having the peripheral region, it is easy to extract the central region as well.

(a) (b) (c) (d) (e)

Fig. 3. Procedure of specifying the central and peripheral region of the lesion: (a) Original mask of the lesion, (b) distance function obtained from the lesion mask, (c) mask of peripheral region (d) mask of central region, and (e) illustrates the points of central (orange circles) and peripheral (blue circles) regions overlying in the original image. Region between these two annotated borders is used for construction of the rubber sheet model, as lines demonstrate the sampling path.

4.2. Daugman's rubber sheet model

For the task of iris recognition, Daugman [20] proposed to project the iris image from Cartesian coordinates to pseudo polar coordinates. With this approach, he achieved an iris representation which is robust against variations in size of iris, size of the pupil, the location of the iris in the image, the relative location of iris and pupil, and orientation of the iris [20]. In analyzing the peripheral region of the skin lesions, these types of robustness are desirable because size, location, orientation and shape of lesions are changing from one image to another

With this assumption that lesion's outer border is analogous to iris border, and the border of lesion's central region (inner border of the peripheral region) being analogous to the border of the pupil, we can define the rubber sheet model as in [20]:

$$I\left(x(r,\theta), y(r,\theta)\right) \rightarrow I\left(r,\theta\right), \tag{4}$$

which maps the image of peripheral regions $I(x,y)$ from Cartesian coordinates to $I(r,\theta)$ which is dimensionless polar coordinates. In the above mapping, $x(r,\theta)$ and $y(r,\theta)$ are Cartesian locations from peripheral region and based on [20] are defined as a linear combination of the central region boundary points $(x_c(r,\theta), y_c(r,\theta))$ and their corresponding points on the outer boundary of the peripheral region $(x_p(r,\theta), y_p(r,\theta))$ in radial direction:

$$\begin{aligned} x(r,\theta) &= (1-r)x_c(\theta) + rx_p(\theta), \\ y(r,\theta) &= (1-r)y_c(\theta) + ry_p(\theta), \end{aligned} \tag{5}$$

where, r is in the range of $[0,1]$, and θ in between $[0,2\pi]$.

In a simple word, we try to sample the pixel values of the lesion image in the peripheral region to construct a rubber sheet model (see Fig. 3-(e) and Fig. 4 for illustration). In this article, we set the number of angular sampling to 360, and the number of radial sampling on each line was set 180 points. Therefore, the obtained rubber sheet model would be like a rectangular image having 180 rows and 360 columns. It is worth mentioning that we use nearest neighbors interpolation to sample the pixel values. This transformation can also transfer the radial structures in the texture to a vertical representation. This can help to better describe the streak like structures in the peripheral regions. To better illustrate this fact, we apply this mapping on a synthetic phantom image of a lesion with exaggerated streak like structures in it and report the result of the transformation in Fig. 4. As you can see all structures that were previously oriented in radial fashion are now oriented vertically in the mapped image. In Fig. 5 two instances of the introduced mapping for two different lesions are shown. As one can see, texture appearance in rubber sheet model depends on the lesion texture in the peripheral region, and it is obvious that radial texture structures became vertical in the transformed image. The latter property can help us in analyzing the dermoscopic structures like streaks as they all take vertical orientation in the new pseudo polar space. Having a mapped image with the same size for all lesions facilitate the procedure of textural feature extraction. In the next subsections, we will introduce some features that can express the texture of Daugman's model.

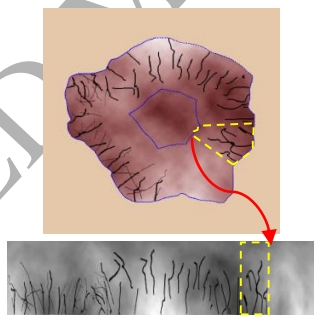

Fig. 4. Daugman's rubber sheet model from peripheral region of a synthetic phantom image.

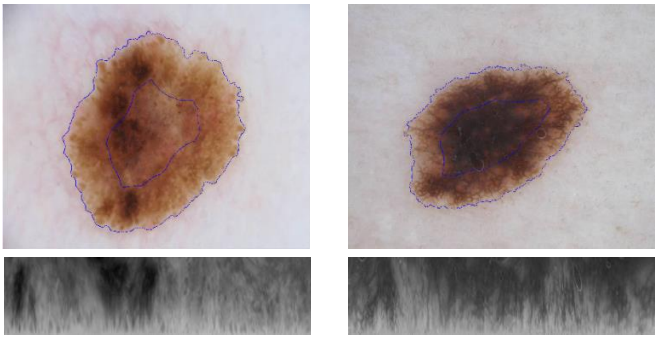

Fig. 5. Two instances of applying the Daugman transformation on real dermoscopic images.

4.3. Textural features to characterize Daugman's model

The obtained rubber sheet model is like a rectangular image for each lesion, therefore, there can't be any shape features for that. The same is true for the color features because the Daugman's model is obtained from just a single channel image (L from La*b*). Hence, we only analyzed the texture of rubber sheet model.

4.3.1. Gray-level run-length matrix features (11 features)

Features that are based on the gray-level run-length matrix (GRLM) mostly characterize the coarseness of image texture. Construction and use of GRLM for feature extraction is like GLCM and done through two phases. First run-length matrix is constructed by counting the number of pixel sequences that are oriented at a particular angle and have a continuous repetition of a specific gray-level value. Second, textural features are extracted based on the constructed GRLM. Having a longer run-length of pixels that share a similar value represents a coarser texture, and vice versa, a fine texture leads to smaller run-lengths [43]. With this in mind, the GRLM in the orientation of θ is constructed which its $R_\theta(v,r)$ element accounts for the number of repetition of a pixel sequence that is oriented at an angle of θ, has its all pixel values equal to v, and it stands out for the length of r. In practice, we quantize the image to 128 different gray-levels for speed and efficiency purposes [43]. Also, we are only interested in vertical structures in the Daugman's model, so we construct the GRLM in the angle of $\theta = 90°$ only.

Features extracted from GRLM in this article are [43]: Short Run Emphasis (SRE), Long Run Emphasis (LRE), Gray-Level Nonuniformity (GLN), Run Length Nonuniformity (RLN), Run Percentage (RP), Low Gray-Level Run Emphasis (LGRE), High Gray-Level Run Emphasis (HGRE), Short Run Low Gray-Level Emphasis (SRLGE), Short Run High Gray-Level Emphasis (SRHGE), Long Run Low Gray-Level Emphasis (LRLGE), and Long Run High Gray-Level Emphasis (LRHGE). For the sake of familiarity, one of these features is described below, for the exact definition of other ten features please refer to [43]. Short Run Low Gray-Level Emphasis (SRLGE) can be defined using (6), in which L is the number of gray levels and N_r is the maximum run-length;

$$SRLGE = \frac{1}{K}\sum_{v=1}^{L}\sum_{r=1}^{N_r}\frac{R(a,r)}{a^2 r^2}, \qquad K = \sum_{v=1}^{L}\sum_{r=1}^{N_r} R(a,r). \tag{6}$$

4.3.2. Edge frequency (1 feature)

Power of the edges in the mapped image from the peripheral region can be a good descriptor for this region. In this section, we mostly look for vertical edges, because dermoscopic features that we are interested in, are rather oriented vertically. More vertical edges imply more vertical structures (like

streaks) in the image. To emphasize on vertical edges, we use the magnitude of the horizontal gradient from the image. For edge frequency, we compute the average over values of gradient magnitude.

4.3.3. Texture fractal dimension (1 feature)

Texture fractal dimension (TFD) is a statistical measure to quantify the texture complexity in the image. In a basic form, fractal dimension describes the relationship between the image scale variation and concluded measurements in that scale. A rougher texture in the image would lead to a bigger fractal dimension, and vice versa. To obtain the texture fractal dimension of the lesion, we implement the method of 3D fractal dimension using differential box-counting as described in [44].

So far, we have introduced 90 features in four different categories: 12 shape features, 19 color features, 46 texture features (extracted from the whole lesion area), and 13 features extracted based on Daugman's rubber sheet model (constructed from the peripheral region of the lesion).

5. Results and experimental setups

5.1. Dataset description

In this article, we use PH^2 image dataset [27], which is a free available dataset of dermoscopic images captured at the dermatology service of hospital Pedro Hispano, Matosinhos, Portugal. It comprises a total of 200 dermoscopic images, in which 80 samples are diagnosed as typical naevi, 80 samples as atypical naevi and other 40 samples as melanomas. PH^2 is introduced to serve as a benchmarking dataset in the field of melanoma recognition and several types of research have been applied on it [6,10,14,22,26,33,45], which makes it appropriate for the comparison purposes and evaluating our new approach.

5.2. Evaluation metrics

The metrics that have been used for segmentation and classification methods evaluation are the same in definition and use a similar notation. In other words, we evaluate the segmentation as we evaluate the task of binary classification using accuracy (Acc), sensitivity (Sens), and specificity (Spec) metrics. For evaluation of the segmentation, alongside the above-mentioned metrics, two additional metrics are used. These metrics are Dice similarity coefficient (DSC) and Jaccard similarity Index (JSI) [8].

5.3. Segmentation results

We evaluate the performance of the proposed segmentation method quantitatively and qualitatively. In Table 1 the results of applying the proposed method on the PH^2 dataset are presented alongside with other state-of-the-art algorithms for lesion segmentation. The reported values are the average of segmentation evaluation metrics on 200 images. Silveira et al. proposed several methods for skin lesion segmentation in

[6], here we report their best-performed method which is based on adaptive deformable models (adaptive snakes). The proposed segmentation algorithm achieved the average accuracy of 96.5%. Also, high values of similarity coefficients have been reported for segmentation outputs, i.e. DSC and JSI metrics equal to 92% and 85.8%, respectively. To see the performance of the proposed segmentation algorithm qualitatively, we illustrate the segmentation results for two melanoma and non-melanoma samples in Fig. 6.

Table 1
Evaluation of the proposed segmentation algorithm

Methods	Average of evaluation metrics				
	DSC	JSI	Acc	Sens	Spec
Silveira [6]	0.940	-	-	0.970	0.960
Pennisi [22]	-	-	0.894	0.710	0.971
Barata [11]	0.900	0.837	0.928	0.904	0.970
Our method	0.920	0.858	**0.965**	0.954	**0.981**

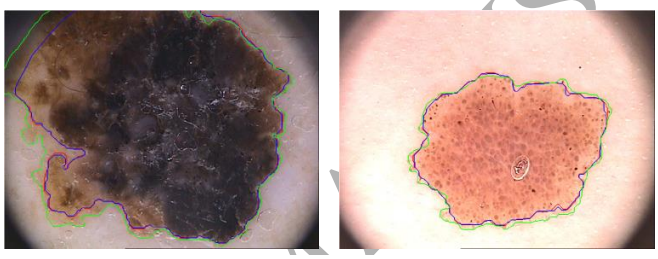

Fig. 6. Two examples of applying the proposed segmentation algorithm on dermoscopic images. The green contours specify the ground truth segmentation, red contours depict the initial segmentation (thresholding) output, and blue contours stand for the proposed segmentation output.

5.4. Classification results

Here we discuss the melanoma recognition as two different binary classification schemes: scheme1) classifying melanoma vs. nevus, and scheme2) classifying melanoma vs. nevus and atypical nevus. For the scheme1 we will have 40 melanoma and 80 nevus samples for which a linear SVM is used for the classification task. The scheme1 can be used to show the discriminative power of the proposed feature set. In the scheme2, 40 melanoma samples are examined alongside with 160 nevus and atypical nevus samples. As you can see, the class population is far more imbalanced in the scheme2, which will arise a problem in using linear SVM, because this classifier is usually biased toward the class with a greater population [21]. To deal with this problem, we use RUSBoost classifier [22]. RUSBoost is proposed to balance the class population by sampling each class in the amount of the population of the smaller class and then train the classifier [22]. However, we use the second scheme to compare our proposed algorithm and features performance with other state-of-the-art methods.

SFS evaluates different features and their combination in a 10-fold cross-validation framework to achieve an optimal set based on a specific criterion. The criterion on which SFS selects the features (sort

out the most important ones) must be picked carefully. Usually, classification accuracy (or classification error rate) is used as SFS criterion. In the current problem and with the available dataset, accuracy is not a fair criterion, because PH^2 dataset has different populations in different categories. So, accuracy criterion may bias the classifier toward the group with more population (normal cases) and hence reduce the sensitivity of recognition. To reduce this unpleasant effect, we propose to use the average of classification sensitivity and specificity as the criterion for SFS experiments. Therefore, SFS will try to maximize the sensitivity and specificity simultaneously. It has been seen that by elevating the sensitivity and specificity, accuracy will increase as well.

Based on the SFS experiments in Fig. 7 and Fig. 9, we select the optimal feature set for each of scheme1 and scheme2 to achieve their best performance. For the shceme1, the linear SVM classifier trained on an optimal feature set with only 4 features was able to achieve an accuracy of 99.2%, sensitivity of 97.5%, and specificity of 100% in the melanoma vs. nevus classification as reported in Tables 2, 3. In the same way for scheme2, using RUSBoost classifier with 8 optimal features will grant all accuracy, sensitivity, and specificity metrics equal to 95% for melanoma vs. nevus and atypical nevus classification as reported in Table 4. In both scheme1 and scheme2, the proposed classification systems outperformed the other state-of-the-art algorithms.

Table 2
The first scheme classification evaluation at different levels of SFS

level	Added feature	Acc	Sens	Spec
1	Daugman's model GRLM: short run low gray-level emphasis	0.900	0.850	0.925
2	Average of channel b* information	0.958	0.925	0.975
3	Energy of lesion's histogram	0.983	0.975	0.987
4	Average of lesion's histogram	0.992	0.975	1.000

Table 3
The First scheme melanoma classification results comparison with the other state-of-the-art algorithms.

Method	Description	Acc	Sens	Spec
Marques [33]	Shape, color, and texture feature + KNN classifier (163 images)	0.791	0.774	0.941
Barata 1 [14]	Bag of features + Dictionary learning (176 images)	-	0.93	0.88
Barata 2 [10]	Bag of features + SVM classifier (102 images)	-	0.93	0.84
Proposed (scheme 1)	Scheme 1 optimal features (four features) + linear SVM classifier (120 images)	**0.992**	**0.975**	**1.000**

Table 4
The second scheme melanoma classification results comparison with the other state-of-the-art algorithms.

Method	Description	Acc	Sens	Spec
Pennisi 2015 [26]	Shape, color, and texture feature + Adaboost classifier	-	0.93	0.85
Pennisi 2016 [22]	More shape, color, and texture feature + Adaboost classifier	-	0.93	0.87
Barata 2017 [46]	Color consistency + bag of features + SVM classifier	0.843	0.925	0.763
Biased classification	Using 33 features + linear SVM classifier	0.955	0.925	96.2
Proposed (scheme 2)	Scheme 2 optimal features (eight features) + RUSBoost classifier	**0.950**	**0.950**	**0.950**

6. Discussion

Based on the results in Table 1, our proposed segmentation method has outperformed the other methods in accuracy and specificity metrics. Method of Silveira [6] reported to has higher DSC (and probably higher JSI) and sensitivity metrics than our method, but it is worth mentioning that Silveira's method is a semi-automatic approach which needs the user to manually specify two regions inside and outside of the lesion [6] while our proposed method is a fully automatic approach and there is no need for the user intervention. Also, the difference in performance of these two methods is only about 0.02 for DSC metric, which can be neglected in practice.

SFS has this nice property to somehow sort the features based on their distinction power. By conducting the first classification scheme (scheme1) experiments on 120 dermoscopic samples, the four most important features that can discriminate between melanoma and nevus are identified and reported in Table 2. In Table 2, "level" column expresses the number of features in the optimal set of selected features (different levels), and the column of "added feature" describes the newly selected feature in that level. SFS has 90 levels (same as the number of features) and reporting the results of all levels in the format of a table is very space consuming, so in the Fig. 7 we plot the curves of classification evaluation metrics vs. the SFS levels.

As you can see in Table 2, by using only 4 features we can achieve the accuracy of 99.2%, sensitivity of 97.5%, and specificity of 100% in distinguishing melanoma from typical naevi. This high level of melanoma recognition can be achieved by incorporating short run low gray-level emphasis derived from Daugman's model GRLM (SRLGE in (6)) alongside with the average of the color pixels of the lesion derived from the b* channel of the La*b* color system, energy and average of the histogram bins (constructed from lesion region). As you can see, SRLGE (which is a textural feature) alone is able to achieve 90% accuracy, 85% sensitivity, and 92.5% specificity in classification of skin lesions, which proves the reliability and distinction power of the newly proposed features based on the peripheral region

information, which are robust against lesion's size, orientation, and color. Adding other three features boosts the metrics to their maximum. As illustrated in Fig. 7, these metrics are still the same until at the level 38 in which metrics start to decrease. Fig. 7 also shows the importance of conducting SFS experiments, as it obvious, in using all extracted features evaluation metrics will end up much worse. In the scheme1 classification task, the optimal selected set of features outperforms the full set of features by a high margin for Specificity: 4%, Sensitivity: 10%, and Accuracy: 6.2%.

To better describe the power of the proposed melanoma recognition system, and prove the discrimination ability of the proposed features, we conduct the second classification scheme (scheme2) in which our target is to recognize melanoma vs. nevus and atypical nevus. This classification scheme suffers from unbalanced class population (40 melanoma samples in one class against 160 nevus and atypical nevus samples in the other class). As we mentioned in the result section, using linear SVM for classifying problems with unbalanced class populations is not desirable because it bias towards the class with bigger population. If melanoma group be the positive class which has the smaller population, this effect would led to decrease in melanoma detection sensitivity. This problem is evident in the SFS curves of Fig. 8, in which the classification specificity is high from the beginning of experiment but sensitivity stays low respectfully. This means that linear SVM has more tendency to classify the samples in non-melanoma group, which is a serious inefficiency. Keep in mind that by adding more features in the SFS experiment, the sensitivity does not reach a favorable value. For example, the optimal performance of linear SVM on scheme2 data achieves 95.5% accuracy, 92.5 sensitivity, 96.2% specificity by using 33 features. However, discriminative power of the proposed features is high enough to make the results of linear SVM on scheme2 comparable to the other state-of-the-art algorithms as reported in fourth row of Table 4.

In order to overcome the problem of unbalanced class population, we proposed to use RUSBoost classifier. By performing SFS experiment on 200 PH^2 samples using RUSBoost classifier, the evaluation metrics will be achieved like the curves in Fig. 9. Based on SFS experiment in Fig. 9, evaluation metrics raise monotonically until the first four features are selected and they start to oscillate afterward. However, it seems that the first 8 selected features can act as the optimal set in this experiment because, at this point for the highest sensitivity of 95%, we can also achieve good enough specificity and accuracy of 95%. These 8 optimal features can be listed as follows: SNR of b* channel, the perimeter of the lesion, GLCM homogeneity, GLCM energy, histogram variance, the energy of first Laws' filter response, GRLM short run emphasis, and GRLM short run low gray-level emphasis (extracted from Daugman's model). Note that the higher fluctuations of the curves in the Fig. 9 in comparison to Fig. 7 is due to the nature of the RUSBoost method. In every feature selection level, a cross-validation experiment is conducted, and in every cross-validation experiment, the RUSBoost algorithm randomly selects a subset of training data in order to balance the population of training classes. This random selection of training data causes the

evaluation metrics on SFS curves oscillating. However, the main trend of the performance curves in Fig. 9 is similar to those in Fig. 7 (first increasing, then fluctuate around some fixed points, and finally decreasing by adding more features). High difference between the performance of scheme2 optimal feature set and full feature set is also clear for this classification scheme (differences are considerable for Specificity: 3%, Sensitivity: 13%, and Accuracy: 5%).

We compare the performance of this set of 8 optimal features with the performance of some state-of-the-art methods in melanoma recognition task. Results of this comparison study are available in Table 4. A full description of other methods is beyond the scope of this article, but a brief description of each of them can be found in the Tables 3, 4, and also in the introduction section. It is important to note that only the methods that have been mentioned in Table 4 used the exact number of 200 dermoscopic images in their dataset and therefore it is only fair to compare the results of scheme2 with them, rest of the studies chose a subset of images to experiment their methods on them (number of samples used in each method is given in the description column). Based on the comparison in Table 4, our proposed set of 8 optimal features used alongside with RUSBoost classifier outperforms the other state-of-the-art methods with a high margin. In comparison to other algorithms, our method achieves better classification results on melanoma vs. nevus recognition using only 4 features (Table 3). These results show the high distinction power of the proposed set of features based on the information from peripheral regions of the lesion.

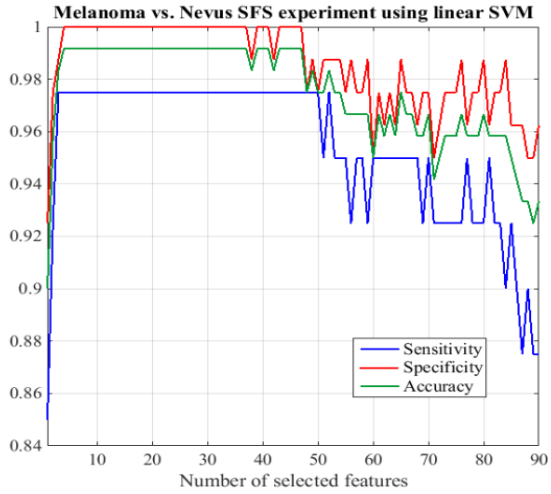

Fig. 7. Curves of classification performance metrics (accuracy, sensitivity, and specificity) through different levels of SFS in the first classification scheme (melanoma vs. nevus) using linear SVM classifier.

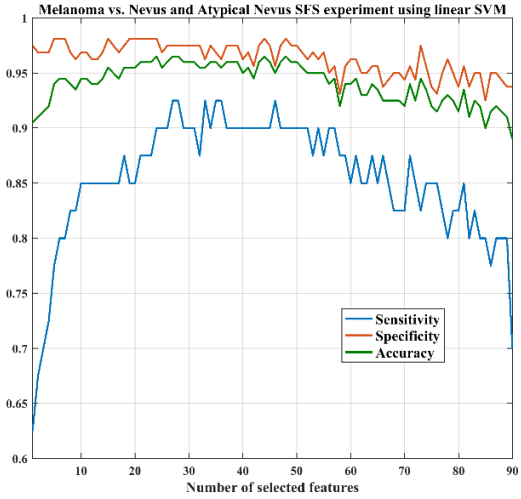

Fig. 8. Curves of classification performance metrics (accuracy, sensitivity, and specificity) through different levels of SFS in the second classification scheme (melanoma vs. nevus and atypical nevus) using linear SVM classifier.

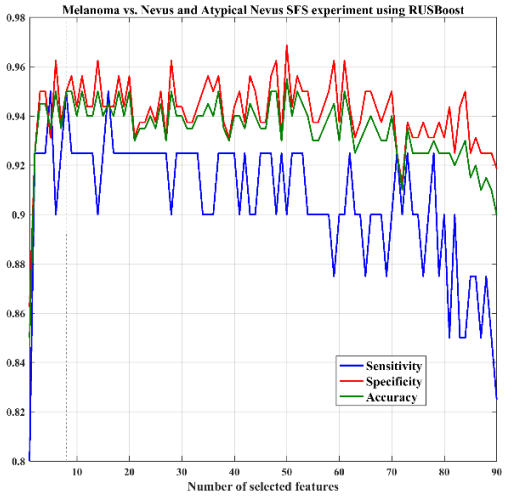

Fig. 9. Curves of classification performance metrics (accuracy, sensitivity, and specificity) through different levels of SFS in the second classification scheme (melanoma vs. nevus and atypical nevus) using RUSBoost classifier.

7. Conclusion and future works

In this paper, we proposed a fully automatic approach to classify melanoma lesions from nevus and atypical nevus in the dermoscopic images. The proposed approach comprises four main steps: preprocessing, segmentation, feature extraction, and feature classification. Preprocessing and segmentation steps have been done based on algorithms in our previous work [9].

The main contribution of this research lied in the feature extraction phase. We proposed to use a set of features globally and locally describing the shape, color, and texture of the lesion. Knowing that

peripheral region of the lesion contains important dermoscopic features (like streaks or pigment networks), we proposed to map pixels of this region from Cartesian space to a pseudo polar space, as done in [20], and called this obtained image as the Daugman's rubber sheet model. Total of 90 features describing the lesion's general shape, color, texture, and also Daugman's model textures were extracted to be used for the lesion classification. To elevate the classification performance, we also proposed to conduct sequential feature selection experiments on the extracted features.

The final task of the system is melanoma recognition or lesion classification. We conducted classification experiments in two different schemes. In the first scheme, melanoma recognition was evaluated (on 120 images in 10-fold cross-validation framework) with an accuracy of 99.2%, the sensitivity of 97.5%, and specificity of 100% by using only 4 features incorporating with the linear SVM classifier. It is worth mentioning that the most important feature was SRLGE from proposed Daugman's model. For the second classification scheme (comprising 8 optimal features alongside with RUSBoost classifier) experiments were conducted on 200 dermoscopic images and we achieved sensitivity, specificity, and accuracy of 95% which surpassed the other state-of-the-art algorithms applied on the same dataset. This fact proved the distinction power of the proposed set of features based on the peripheral image information.

We believe that our new set of features based on the peripheral lesion information can be coupled with other dermoscopic features to train more powerful classifiers for the task of melanoma recognition. It might be a good practice to use deep convolutional neural networks to extract features from the peripheral region's Daugman model and incorporate them in the melanoma recognition system as well (e.g., as a complementary set of features in a fully convolutional neural network recognition approach like [9]). It is also clinically valuable to recognize the type of the streaks in the peripheral region of a lesion i.e., absent, typical, and atypical [15]. It is promising that the proposed set of features based on the Daugman's rubber sheet model can elevate the performance in that area as well.

REFERENCES

[1] The American Cancer Society medical and editorial content team, Key Statistics for Melanoma Skin Cancer, Am. Cancer Soc. (2017).

[2] B.W. Stewart, C.P. Wild, World Cancer Report 2014, World Health Organization, 2014. doi:9283204298.

[3] T. Celebi, M. Emre; Marques, Jorge S.; Mendonca, Dermoscopy image analysis, (Digital imaging and computer vision series), 1st ed., CRC Press LLC, 2016.

[4] K. Korotkov, R. Garcia, Computerized analysis of pigmented skin lesions: a review., Artif. Intell. Med. 56 (2012) 69–90. doi:10.1016/j.artmed.2012.08.002.

[5] I. Maglogiannis, C.N. Doukas, S. Member, Overview of Advanced Computer Vision Systems for Skin Lesions Characterization, IEEE Trans. Inf. Technol. Biomed. 13 (2009) 721–733.

[6] N.K. Mishra, M.E. Celebi, An Overview of Melanoma Detection in Dermoscopy Images Using Image Processing and Machine Learning, arXiv Prepr. arXiv1601.07843. (2016) 1–15.

[7] M. Silveira, J.C. Nascimento, J.S. Marques, A.R.S. Marçal, T. Mendonça, S. Yamauchi, J. Maeda, J. Rozeira, Comparison of segmentation methods for melanoma diagnosis in dermoscopy images, Sel. Top. Signal Process. IEEE J. 3 (2009) 35–45.

[8] R.B. Oliveira, E. Mercedes Filho, Z. Ma, J.P. Papa, A.S. Pereira, J.M.R.S. Tavares, Computational methods for the image segmentation of pigmented skin lesions: a review, Comput. Methods Programs Biomed. 131 (2016) 127–141.

[9] N. Zamani Tajeddin, B. Mohammadzadeh Asl, A General Algorithm for Automatic Lesion Segmentation in Dermoscopy

Images, in: 23th Natl. 1st Int. Iran. Conferance BioMediacal Eng., Tehran, 2016: pp. 134–139. doi:10.1109/ICBME.2016.7890944.
[10] A. Sáez, B. Acha, C. Serrano, Pattern Analysis in Dermoscopic Images, in: J. Scharcanski, M.E. Celebi (Eds.), Comput. Vis. Tech. Diagnosis Ski. Cancer, Ser. Bioeng., Springer Berlin Heidelberg, Berlin, Heidelberg, 2014: pp. 23–48. doi:10.1007/978-3-642-39608-3.
[11] C. Barata, M. Ruela, M. Francisco, T. Mendonça, J.S. Marques, Two Systems for the Detection of Melanomas in Dermoscopy Images Using Texture and Color Features, IEEE Syst. J. 8 (2013) 965–979.
[12] M. Rastgoo, R. Garcia, O. Morel, F. Marzani, Automatic differentiation of melanoma from dysplastic nevi., Comput. Med. Imaging Graph. 43 (2015) 44–52. doi:10.1016/j.compmedimag.2015.02.011.
[13] K. Shimizu, H. Iyatomi, M.E. Celebi, K.-A. Norton, M. Tanaka, Four-class classification of skin lesions with task decomposition strategy., IEEE Trans. Biomed. Eng. 62 (2015) 274–83. doi:10.1109/TBME.2014.2348323.
[14] C. Barata, J.S. Marques, J. Rozeira, The role of keypoint sampling on the classification of melanomas in dermoscopy images using bag-of-features, in: Iber. Conf. Pattern Recognit. Image Anal., Springer, Berlin, Heidelberg, 2013: pp. 715–723.
[15] M. Sadeghi, T.K. Lee, D. McLean, H. Lui, M.S. Atkins, Detection and Analysis of Irregular Streaks in Dermoscopic Images of Skin Lesions, IEEE Trans. Med. Imaging. 32 (2013) 849–861. doi:10.1109/TMI.2013.2239307.
[16] J.L. García Arroyo, B. García Zapirain, Detection of pigment network in dermoscopy images using supervised machine learning and structural analysis., Comput. Biol. Med. 44 (2014) 144–57. doi:10.1016/j.compbiomed.2013.11.002.
[17] I. Maglogiannis, K.K. Delibasis, Enhancing classification accuracy utilizing globules and dots features in digital dermoscopy., Comput. Methods Programs Biomed. 118 (2015) 124–33. doi:10.1016/j.cmpb.2014.12.001.
[18] M.E. Celebi, H. Iyatomi, W. V Stoecker, R.H. Moss, H.S. Rabinovitz, G. Argenziano, H.P. Soyer, Automatic detection of blue-white veil and related structures in dermoscopy images, Comput. Med. Imaging Graph. 32 (2008) 670–677.
[19] R.B. Oliveira, A.S. Pereira, J.M.R.S. Tavares, Skin lesion computational diagnosis of dermoscopic images: Ensemble models based on input feature manipulation, Comput. Methods Programs Biomed. 149 (2017) 43–53.
[20] J. Daugman, How Iris Recognition Works, IEEE Trans. Circuits Syst. Video Technol. 14 (2004) 21–30. doi:http://dx.doi.org/10.1016/B978-012119792-6/50133-9.
[21] C.M. Bishop, Pattern recognition and machine learning, springer New York, 2006.
[22] C. Seiffert, T.M. Khoshgoftaar, J. Van Hulse, A. Napolitano, RUSBoost: A hybrid approach to alleviating class imbalance, IEEE Trans. Syst. Man, Cybern. A Syst. Humans. 40 (2010) 185–197.
[23] A. Pennisi, D.D. Bloisi, D. Nardi, A.R. Giampetruzzi, C. Mondino, A. Facchiano, Skin lesion image segmentation using Delaunay Triangulation for melanoma detection, Comput. Med. Imaging Graph. 52 (2016) 89–103. doi:10.1016/j.compmedimag.2016.05.002.
[24] Q. Abbas, I. Fondón, M. Rashid, Unsupervised skin lesions border detection via two-dimensional image analysis, Comput. Methods Programs Biomed. 104 (2010) e1–e15. doi:10.1016/j.cmpb.2010.06.016.
[25] P.G. Cavalcanti, J. Scharcanski, A coarse-to-fine approach for segmenting melanocytic skin lesions in standard camera images, Comput. Methods Programs Biomed. 112 (2013) 684–693. doi:10.1016/j.cmpb.2013.08.010.
[26] M. Jahanifar, N. Zamani Tajedddin, B. Mohammadzadeh Asl, A. Gooya, Supervised Saliency Map Driven Segmentation of the Lesions in Dermoscopic Images, arXiv Prepr. arXiv1703.00087v3. (2017) 1–10.
[27] A. Pennisi, D.D. Bloisi, D. Nardi, A.R. Giampetruzzi, C. Mondino, A. Facchiano, Melanoma Detection Using Delaunay Triangulation, (n.d.). doi:10.1109/ICTAI.2015.117.
[28] T. Mendonça, P.M. Ferreira, J.S. Marques, A.R.S. Marcal, J. Rozeira, PH2 - A dermoscopic image database for research and benchmarking, in: 35th Annu. Int. Conf. IEEE Eng. Med. Biol. Soc., 2013: pp. 5437–5440. doi:10.1109/EMBC.2013.6610779.
[29] T. Lee, V. Ng, R. Gallagher, A. Coldman, D. McLean, Dullrazor®: A software approach to hair removal from images, Comput. Biol. Med. 27 (1997) 533–543. doi:http://dx.doi.org/10.1016/S0010-4825(97)00020-6.
[30] A. Oppenheim, R. Schafer, T. Stockham, Nonlinear filtering of multiplied and convolved signals, IEEE Trans. Audio Electroacoust. 16 (1968) 437–466. doi:10.1109/TAU.1968.1161990.
[31] N. Otsu, A Threshold Selection Method from Gray-Level Histograms, IEEE Trans. Syst. Man. Cybern. 9 (1979) 62–66. doi:10.1109/TSMC.1979.4310076.
[32] R. Malladi, J.A. Sethian, B.C. Vemuri, Shape modeling with front propagation: A level set approach, IEEE Trans. Pattern Anal. Mach. Intell. 17 (1995) 158–175.
[33] Y. (Iris) Cheng, R. Swamisai, S.E. Umbaugh, R.H. Moss, W. V Stoecker, S. Teegala, S.K. Srinivasan, Skin lesion classification using relative color features, Ski. Res. Technol. 14 (2008) 53–64. doi:10.1111/j.1600-0846.2007.00261.x.
[34] J.S. Marques, C. Barata, T. Mendonça, On the role of texture and color in the classification of dermoscopy images, in: 2012 Annu. Int. Conf. IEEE Eng. Med. Biol. Soc., IEEE, 2012: pp. 4402–4405.
[35] H. Ganster, A. Pinz, R. Röhrer, E. Wildling, M. Binder, H. Kittler, Automated melanoma recognition, Med. Imaging, IEEE Trans. 20 (2001) 233–239.
[36] M.C. Mihm, T.B. Fitzpatrick, M.M.L. Brown, J.W. Raker, R.A. Malt, J.S. Kaiser, Early Detection of Primary Cutaneous Malignant Melanoma: a color atlas, N. Engl. J. Med. 289 (1973) 989–996. doi:10.1056/NEJM197311082891901.
[37] K.I. Laws, Rapid texture identification, in: 24th Annu. Tech. Symp., International Society for Optics and Photonics, 1980: pp. 376–381.
[38] K. Nie, J.-H. Chen, H.J. Yu, Y. Chu, O. Nalcioglu, M.-Y. Su, Quantitative Analysis of Lesion Morphology and Texture Features for Diagnostic Prediction in Breast MRI, Acad. Radiol. 15 (2008) 1513–1525. doi:10.1016/j.acra.2008.06.005.
[39] R.M. Haralick, K. Shanmugam, Textural features for image classification, IEEE Trans. Syst. Man. Cybern. SMC-3 (1973)

610–621.
[40] D.A. Clausi, An analysis of co-occurrence texture statistics as a function of grey level quantization, Can. J. Remote Sens. 28 (2002) 45–62.
[41] L.-K. Soh, C. Tsatsoulis, Texture analysis of SAR sea ice imagery using gray level co-occurrence matrices, IEEE Trans. Geosci. Remote Sens. 37 (1999) 780–795.
[42] G. Chandrashekar, F. Sahin, A survey on feature selection methods, Comput. Electr. Eng. 40 (2014) 16–28. doi:Doi 10.1016/J.Compeleceng.2013.11.024.
[43] X. Tang, Texture information in run-length matrices, IEEE Trans. Image Process. 7 (1998) 1602–1609. doi:10.1109/83.725367.
[44] R.A. Boby, M. Hanmandlu, A. Sharma, M. Bindal, Extraction of fractal dimension for iris texture, in: Biometrics (ICB), 2012 5th IAPR Int. Conf., IEEE, 2012: pp. 330–335.
[45] T. Mendonça, P.M. Ferreira, J.S. Marques, A.R.S. Marcal, J. Rozeira, PH^2 - A dermoscopic image database for research and benchmarking, 2013 35th Annu. Int. Conf. IEEE Eng. Med. Biol. Soc. (2013) 5437–5440. doi:10.1109/EMBC.2013.6610779.
[46] C. Barata, M.E. Celebi, J.S. Marques, Improving dermoscopy image classification using color constancy, IEEE J. Biomed. Heal. Informatics. 19 (2015) 1146–1152.